MODELING OF GALILEO/NIMS EUROPA SPECTRA OF THE ANTI-JOVIAN AND TRAILING SIDESUSING TWO ENDMEMBERS AND WATER ICE

G. B. Hansen

Department of Earth and Space Science, University of Washington, Seattle, WA 98195, USA (ghansen@ess.washington.edu)

Abstract

The Near Infrared Mapping Spectrometer (NIMS) observations at wavelengths 0.7-5.3 µm of the Jovian moon Europa are being reprocessed using information gained throughout and beyond the Galileo mission. Early analysis of these reprocessed data (three observations, including a global scale one of the anti-Jovian and trailing hemispheres at 47 km spatial resolution) show evidence of spectral features not or only weakly apparent before [1]. These include strong absorption bands attributed to CO_2 and SO_2 (centered near 4.25 and 4.0 µm, respectively). The strong hydrate bands, including at near 1.5 and 1.95 µm, are now more clearly defined. The largest amounts of CO_2 and the most well defined hydrate bands are strongly associated with the (endogenic) dark reddish regions on the surface [1, 2]. We will present modeling results from this observation similar to that presented over a year ago using a newly calibrated orbit 1 observation.

Introduction

Europa is the second outward from Jupiter of the four Galilean satellites. It is similar in size to the Earth's moon, and has a young crater-free surface. The interior has a dense rocky/metallic core surrounded by a low density shell 80-170 km thick that is assumed to be primarily ice and/or water. The magnetic signature of Europa implies the presence of a conducting liquid subsurface ocean. Additionally, spectra from Galileo/NIMS showed the surface to be partly covered by heavily hydrated materials such as sulfate salts [3, 4] and/or sulfuric acid hydrate [5, 6]. The hydrated material is concentrated in the regions of darker brownish coloring that occur in some chaos regions and along linea, and may be linked to possible endogenic materials from the subsurface [3].

This Observation

The NIMS builds up spectral images by recording a spectrum over 20 mirror positions and up to 408 wavelengths. These wavelengths are sensed by 17 discrete detectors, each of which covers a small region of the spectrum. The third dimension of the spectral image is filled out by scanning the instrument field-of-view slowly perpendicular to the mirror motion [7]. The NIMS observations of the icy satellites are now being reexamined and recalibrated using new techniques [8, 9, 10]. The Europa observations needed an improved despiking process for the spectra longer than 3 µm, where radiation spikes outnumber the good data by a ratio of 2:1, or more. The first Europa observation to be processed was TERINC (Terra Incognito) from the E6 orbit, which was known to have fewer spikes overall than average. This is a global scale observation with a pixel scale of 47 km

This observation was dark-corrected and radiometrically calibrated using the best dark and calibration values and wavelength list [11]. The wavelengths up to 2.4 µm were despiked using our usual procedure [12]. The short wavelength process yielded about 20% spikes. For the wavelengths longer than about 2.75 ?m the same despiking was used with much tighter parameters. This despiking was repeated three times to remove most of the visible spikes. Then a few hundred remaining small spikes were manually removed up to 4.4 ?m. Beyond this wavelength the spectra have just a few digital numbers (DN) of signal, and contain no information other than a general shape. These wavelengths were constrained to be near spectra from areal averages [1]. The final frequency of spikes in this region was 70-80%.

Three additional Europa data sets were calibrated, SUCOMP2 (pixel scale 7.5 km) [2] from orbit 6, LINEA (pixel scale 17 km) from orbit 3, and NHILAT (pixel scale 79 km) [13] from orbit 1. Both have considerable amounts of dark hydrate, but both have a spike abundance of 80-90% in the longwave part that region from detailed analysis. Due to illness in the last several months, I was only able to complete the modeling of the TERINC observation.

Newly Calibrated and Modeled Observations

Using the model developed for the NHILAT cube [13], we modeled the TERINC observation. A map of the prime mission observations (with this observation the large one outlined in orange) is shown in Figure 1. A monochrome image of the cube with approximate photometric correction and a labelled lat-lon grid is shown in Figure 2. The calibration and projection were complicated by the fact that the two parts of the cube were recorded in different gain states and projected separately in the PDS data. We combined the calibrated raw data and projected them together.

Figure 1

NIMS Europa Primary Mission Coverage (>90 wavelengths)

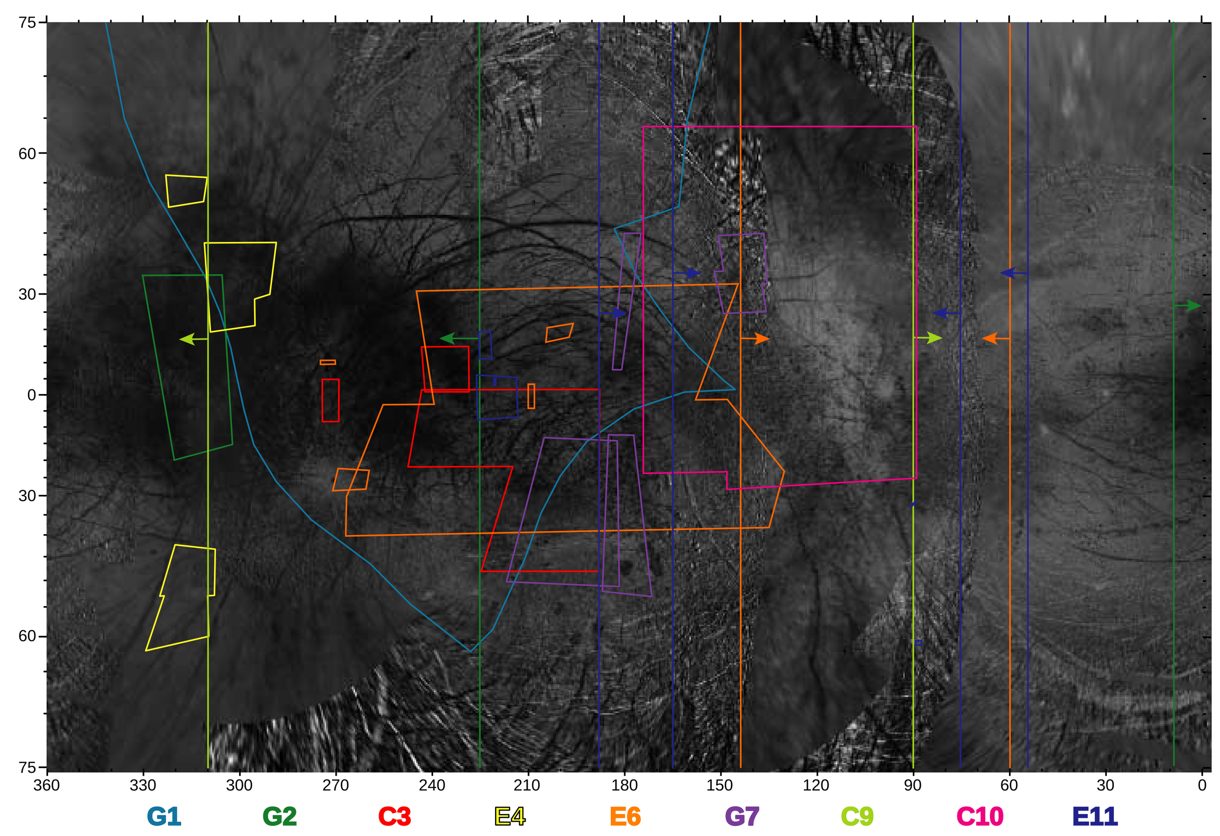

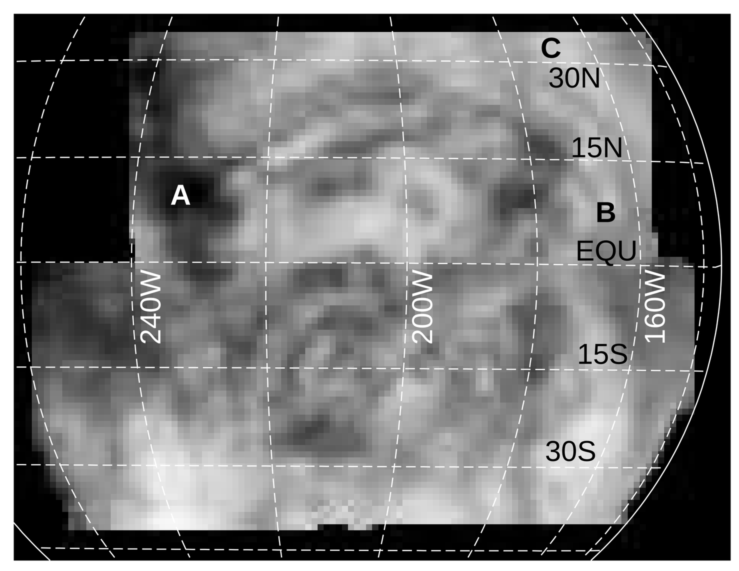

Figure 2

An image at 0.7 µm of the E6TERINC observation with a photometric correction. The extended dark areas show up well, and some of dark linea are resolved.

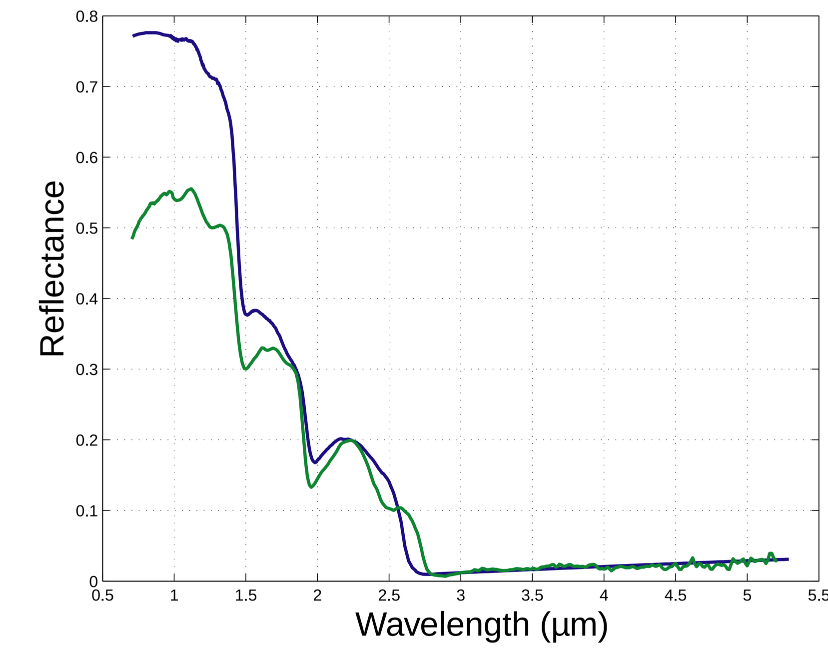

Figure 3

Spectral endmembers used in the modeling. The green spectrum is the Europa hydrate average and the blue spectrum is sulfuric acid hydrate with data extended below 1 µm and above 2.5 µm from [5, 6].

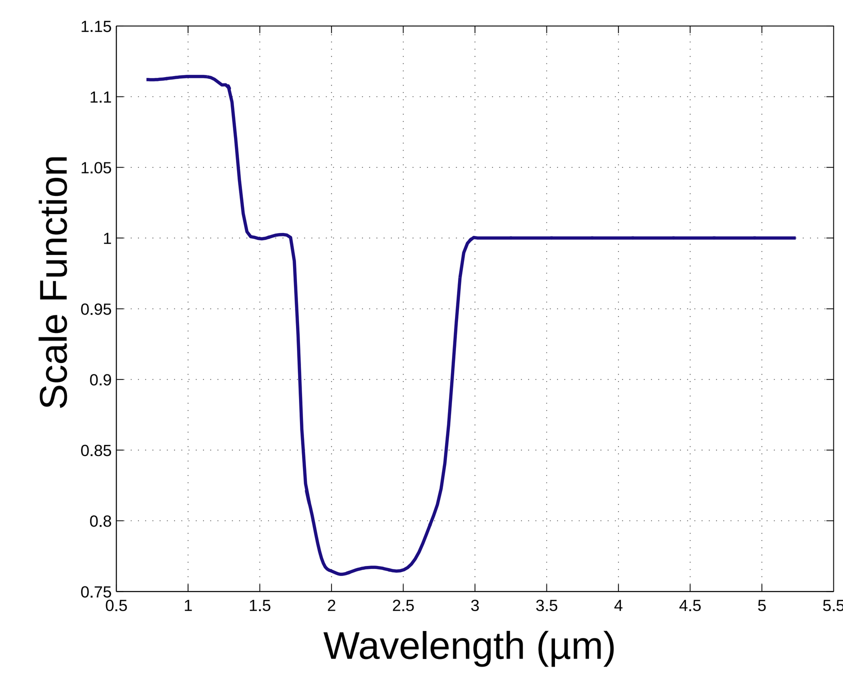

Figure 4

Scaling function taken to a power (-0.5 to ~1.0) and multiplied by the average hydrate to imrove the fits

Modeling the Data

We performed linear modeling of E6TERINC along the lines of [13, 14], using two hydrates and water ice of various grain sizes. The first hydrate was taken from the data, equivalent to the "average" hydrate spectrum from [3] (Figure 3). In additon we used a wavelength-extended version of sulfuric acid hydrate from [5, 6] (Figure 3). A scaling function taken to a variable power is used to modify the average hydrate spectrum to account for photometric variation (Figure 4). A bidirectional reflectance model for water ice (at a temperature of 110 K) with 10 grain sizes was created for the lighting geometry of the cube as a third component.

Modeling Results

The linear modeling of E6TERINC produced very good fits in general. The map of the average hydrate is shown in Figure 5, reaching near unity at some places in the observation. This component is smallest towards the poles. The sulfuric acid hydrate (Figure 6) is present on the trailing side but is strongest (max ~35%) in the mid latitude areas east of 210 W longitude. Water ice is most abundant in the polar regions reaching over 60% there (Figure 7). Figure 8 shows the water ice grain radius (in the upper right corner, the fit is improved by using a mixture of two disparate grain sizes, the largest one near a radius of 1 mm) is largest on parts of the trailing hemisphere (~1 mm), and is smallest towards the leading hemisphere (10-20 µm). The scale factor exponent varies from -1 to 1.5 over the image, generally the highest on the left side and lowest on the right side. A couple of spectral fits spanning the full least squares range of 0.015 to 0.15 are shown in Figures 9 and 10. The misfits on the right side are mostly caused by long-wavelength water ice features that are stronger in the model than the data.

Figure 5

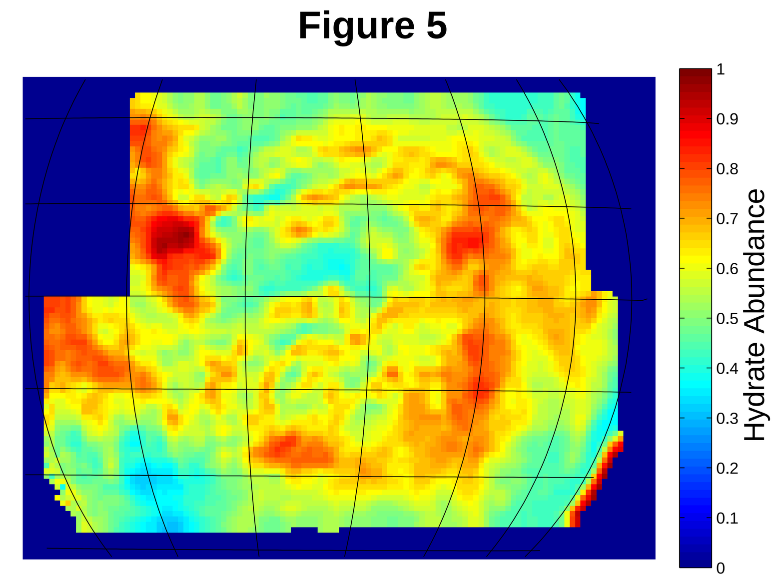

Figure 6

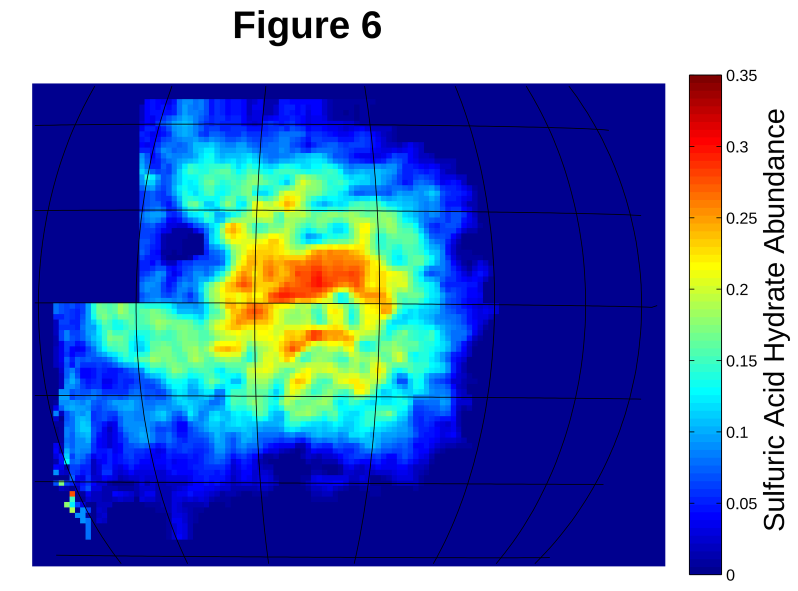

Figure 7

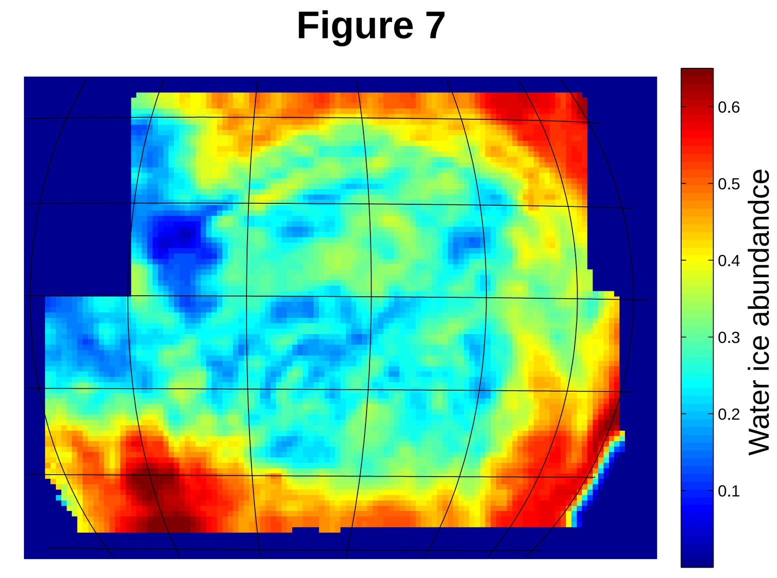

Figure 8

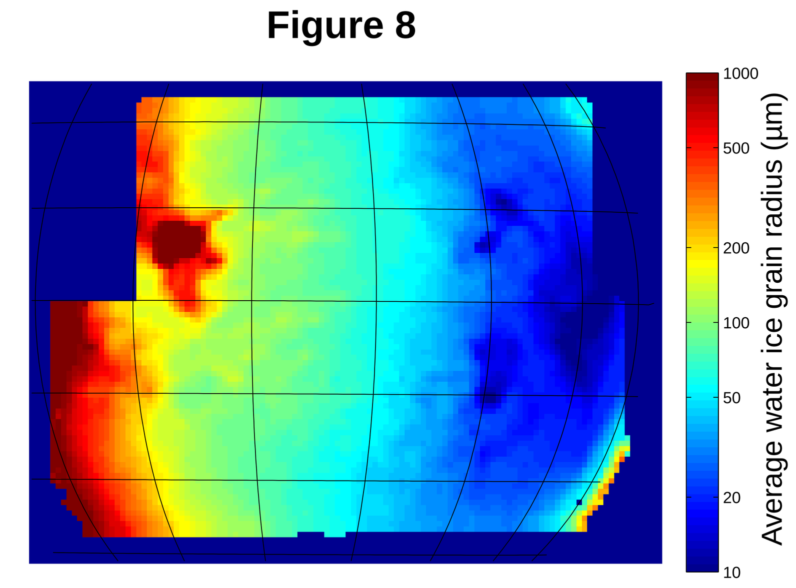

Figure 9: Good fit

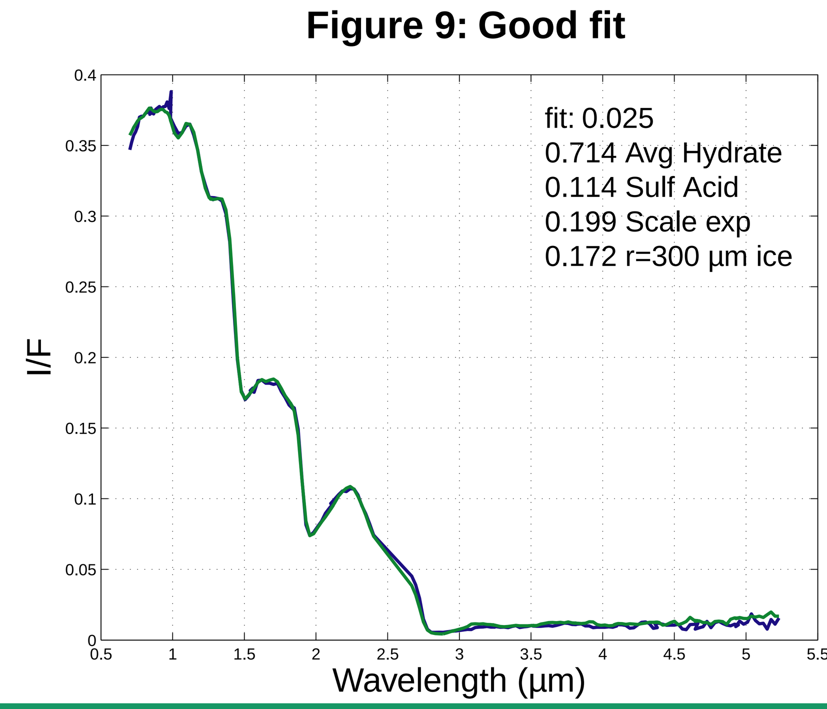

Figure 10: Bad fit

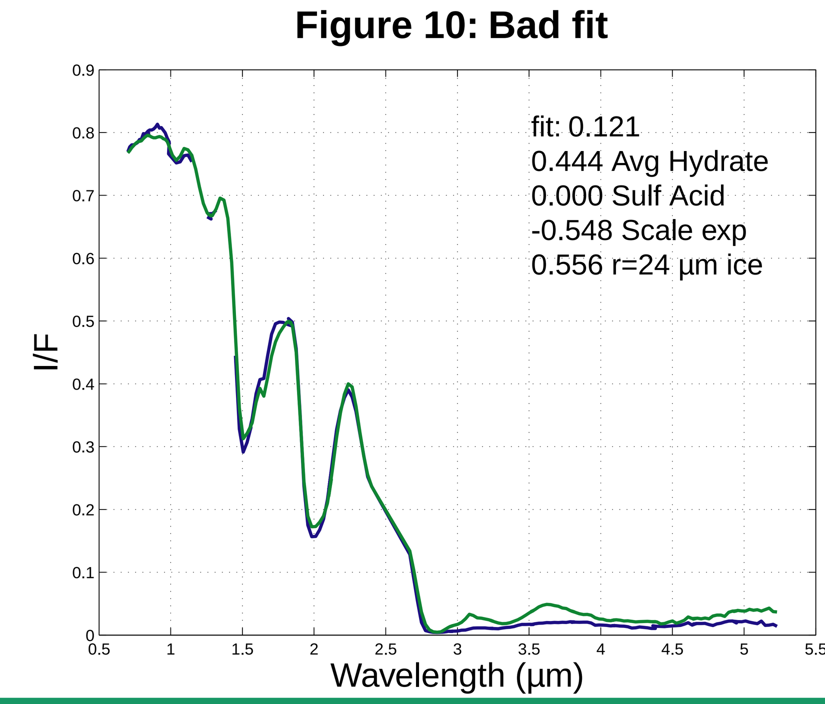

Conclusions and future work

The modeling of this second Europa NIMS cube was straightforward and produced a good result. Our modeling provides good fits with only two non-ice endmembers and a simple scaling factor. The results are generally consistant with similar areas in G1NHILAT, although the higher spatial resolution reveals finer features. The water ice is abundant in the polar regions, less abundant and fine-grained on the leading side and least abundant and large-grained on the trailing side. The average hydrate is abundant on the trailing side and in linea on the anti-Jovian side, and the sulfuric acid hydrate appears on the trailing hemisphere non polar regions, but more abundant on more ice rich regions. Since the sulfuric acid is made by the reaction of sulfur ions and ice, it makes sense that it is more abundant in icy regions. The nature of the endmembers may be revealed by high spatial resolution spectra from a future mission such as the Europa Clipper.

REFERENCES

[1] Hansen, G. B., and McCord, T. B., Geophys. Res. Lett., 35, L01202, doi: 10.1029/2007GL031748, 2008.

[2] McCord, T. B., Hansen, G. B., Combe, J.-P., and Hayne, P., Icarus, 209, 639-650, doi: 10.1016/j.icarus.2010.05.026, 2010.

[3] McCord, T. B., et al., J. Geophys. Res., 104, 11,827-11,852, 1999.

[4] McCord, T. B., Teeter, G., Hansen, G. B., Sieger, M. T., and Orlando, T. M., J. Geophys. Res, 107(E1), 5004, 10.1029/2000JE001453, 2002.

[5] Carlson, R. W., Johnson, R. E., and Anderson, M. S., Science, 286, 97-99, 1999.

[6] Carlson, R. W., Anderson, M. S., Mehlman, R., and Johnson, R. E., Icarus, 177, 461-471, doi: 10.1016/j.icarus.2005.03.026, 2005.

[7] Carlson R. W.,Weissman, P. R., Smythe, W. D., Mahoney, J. C., and The NIMS Science and Engineering Team, Space Sci. Rev., 60, 457-502, 1992.

[8] Hansen, G. B., and McCord, T. B., J. Geophys. Res., 109, E01012, doi: 10.1029/2003JE002149, 2004.

[9] Hansen, G. B., McCord, T. B., Hibbitts, C. A., and Kamp, L. W. (abstract), Bull. Am. Astron. Soc., 38, 540, 2006.

[10] Hansen, G. B., and McCord, T. B (abstract), Bull. Am. Astron. Soc., 40, 506-507, 2008.

[11] McCord, T. B., Hansen, G. B., Shirley, J. H., and Carlson, R. W., J. Geophys. Res., 104, 27,157-27,162, 1999.

[12] Hibbitts, C. A., McCord, T. B., and Hansen, G. B., J. Geophys. Res., 105, 22,541-22,557, 2000.

[13] Hansen, G. B. (abstract), EPSC-DPS2011-589, 2011, EPSC-DPS Joint Meeting 2011, Nantes, France.

[14] Shirley, J. H., Dalton, J. B., Prockter, L. M. and Kamp, L. W., Icarus, 210, 358-384, doi:10.1016/j.icarus.2010.06.018, 2010.